BIOCHEMISTRY
including biophysical chemistry & molecular biology

Article

pubs.acs.org/biochemistry

Kinetic Analysis of 3′−5′ Nucleotide Addition Catalyzed by Eukaryotic tRNA^{His} Guanylyltransferase

Brian A. Smith and Jane E. Jackman*

Department of Biochemistry, Center for RNA Biology and Ohio State Biochemistry Program, The Ohio State University, Columbus, Ohio 43210, United States

Supporting Information

ABSTRACT: The tRNA^{His} guanylyltransferase (Thg1) catalyzes the incorporation of a single guanosine residue at the −1 position (G_{-1}) of tRNA^{His}, using an unusual 3′−5′ nucleotidyl transfer reaction. Thg1 and Thg1 orthologs known as Thg1-like proteins (TLPs), which catalyze tRNA repair and editing, are the only known enzymes that add nucleotides in the 3′−5′ direction. Thg1 enzymes share no identifiable sequence similarity with any other known enzyme family that could be used to suggest the mechanism for catalysis of the unusual 3′−5′ addition reaction. The high-resolution crystal structure of human Thg1 revealed remarkable structural similarity between canonical DNA/RNA polymerases and eukaryotic Thg1; nevertheless, questions regarding the molecular mechanism of 3′−5′ nucleotide addition remain. Here, we use transient kinetics to measure the pseudo-first-order forward rate constants for the three steps of the G_{-1} addition reaction catalyzed by yeast Thg1: adenylylation of the 5′ end of the tRNA (k_{aden}), nucleotidyl transfer (k_{ntrans}), and removal of pyrophosphate from the G_{-1}-containing tRNA (k_{ppase}). This kinetic framework, in conjunction with the crystal structure of nucleotide-bound Thg1, suggests a likely role for two-metal ion chemistry in all three chemical steps of the G_{-1} addition reaction. Furthermore, we have identified additional residues (K44 and N161) involved in adenylylation and three positively charged residues (R27, K96, and R133) that participate primarily in the nucleotidyl transfer step of the reaction. These data provide a foundation for understanding the mechanism of 3′−5′ nucleotide addition in tRNA^{His} maturation.

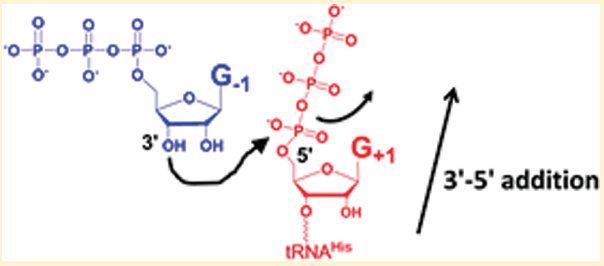

Fidelity of protein synthesis largely depends on the ability of aminoacyl-tRNA synthetases to distinguish between cognate and noncognate tRNA substrates. However, because of the similar secondary and tertiary structures of all tRNAs, proper substrate recognition must be facilitated by identity elements present within the primary sequence of tRNAs. Many characterized identity elements are located in either the anticodon or the aminoacyl-acceptor stem, with the discriminator nucleotide (N_{73}) often playing a significant role.[1]

In most organisms, the histidyl-tRNA synthetase (HisRS) recognizes a single guanosine residue located at the −1 position (G_{-1}) of tRNA^{His} as a critical identity element.[2−7] In *Escherichia coli*, G_{-1} is genomically encoded and retained in the primary transcript following ribonuclease P (RNase P) cleavage of the 5′ leader sequence from the precursor tRNA^{His}; a similar mechanism is predicted to incorporate G_{-1} in most bacteria and some archaea.[8] Cleavage of the pre-tRNA in this case results in a 5′-monophosphorylated tRNA^{His} containing a G_{-1}:C_{73} Watson−Crick (WC) base pair. However, in eukaryotes, the G_{-1} residue is not genomically encoded, and therefore, this mechanism of incorporating the G_{-1} identity element cannot be used. Instead, G_{-1} is added post-transcriptionally via an unusual 3′−5′ addition reaction, as first described in *Schizosaccharomyces pombe* and *Drosophila melanogaster*.[9] In these organisms, the additional residue is added opposite a universally conserved adenosine at position 73, resulting in a non-WC G_{-1}:A_{73} base pair at the top of the acceptor stem.

The enzyme that catalyzes post-transcriptional G_{-1} addition, the tRNA^{His} guanylyltransferase (Thg1), was first discovered in *Saccharomyces cerevisiae*, where it was demonstrated that controlled depletion of Thg1 correlates with accumulation of tRNA^{His} lacking G_{-1}, reduction of aminoacylated tRNA^{His}, and unexpected accumulation of m^5C modifications at positions 48 and 50.[10,11] In yeast, the *THG1* gene is essential for optimal growth, although overexpression of HisRS and its cognate tRNA^{His} can suppress the lethal growth phenotype of the yeast deletion strain.[12] In accordance with the essential role for G_{-1} in tRNA^{His} recognition, Thg1 is highly conserved throughout eukaryotes, which nearly all lack a genomically encoded G_{-1} residue.[10] Interestingly, Thg1 orthologs termed Thg1-like proteins (TLPs) have been identified in some bacteria and archaea that also contain a genomically encoded G_{-1}, where TLPs have been implicated in tRNA 5′ end repair reactions.[13−15] The molecular mechanism of Thg1 is of extreme interest because the Thg1 enzymes are the only known enzymes that catalyze nucleotide addition in the 3′−5′

Received: September 5, 2011
Revised: December 2, 2011
Published: December 2, 2011

direction. However, the mechanism of 3′−5′ addition cannot be inferred through identifiable sequence similarity between Thg1 enzymes and members of any other known enzyme family.

Yeast Thg1 (yThg1) adds G_{-1} to a 5′-monophosphorylated $tRNA^{His}$ (p-$tRNA^{His}$) species generated from RNase P cleavage of the precursor tRNA, and selective recognition of $tRNA^{His}$ is ensured through recognition of the His anticodon (GUG).[16] Addition of G_{-1} to the physiologically relevant p-$tRNA^{His}$ substrate proceeds via a three-step reaction (Figure 1A).

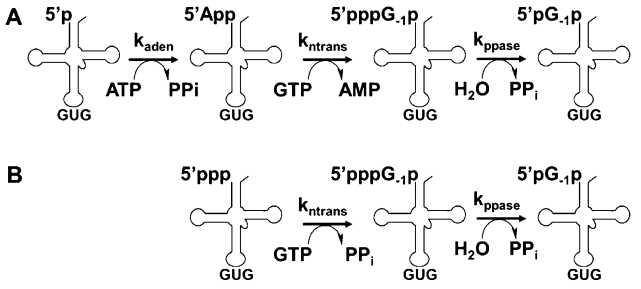

Figure 1. Two pathways for addition of G_{-1} to $tRNA^{His}$. (A) Three-step reaction scheme for addition to the physiologically relevant 5′-monophosphorylated $tRNA^{His}$. (B) Alternative pathway for G_{-1} addition in vitro using a 5′-ppp-$tRNA^{His}$, in which Thg1 bypasses the activation step.

First, yThg1 activates the 5′ end of p-$tRNA^{His}$ using ATP in an adenylylation step, resulting in formation of an adenylylated intermediate (App-$tRNA^{His}$) containing a 5′−5′ phosphoanhydride bond. The presence of the App-activated intermediate was first demonstrated with a partially purified yeast enzyme and confirmed later using purified yThg1, once the identity of the gene was known.[10,17] In both cases, incorporation of [α-^{32}P]AMP from labeled ATP into $tRNA^{His}$ was confirmed by P1 and snake venom nuclease analysis of reaction products, and release of the labeled AMP upon addition of G_{-1} was also demonstrated. In the second step of the G_{-1} addition reaction, yThg1 utilizes the 3′-hydroxyl of GTP to attack the intermediate in a nucleotidyl transfer step, releasing AMP and resulting in addition of a single GTP to the 5′ end of the tRNA ($pppG_{-1}$p-$tRNA^{His}$). Third, yThg1 removes pyrophosphate from the G_{-1} residue in a pyrophosphate removal step, yielding mature pG_{-1}-containing $tRNA^{His}$ (pG_{-1}p-$tRNA^{His}$). Thg1 can also add nucleotides to a 5′-triphosphorylated $tRNA^{His}$ (ppp-$tRNA^{His}$) in the absence of ATP in vitro (Figure 1B).[10] The ppp-$tRNA^{His}$ substrate is presumed to mimic the adenylylated intermediate, allowing Thg1 to bypass the adenylylation step when acting on a substrate containing a preactivated 5′ end.

In addition to non-WC G_{-1} addition that occurs in vivo in yeast with A_{73}-containing $tRNA^{His}$, the natural substrate in eukaryotes, yThg1 also catalyzes multiple rounds of nucleotide addition in a strictly template-dependent 3′−5′ polymerase reaction with a C_{73}-containing $tRNA^{His}$ variant in vitro.[18] This reverse polymerase activity forms G:C and C:G WC base pairs, and while yThg1 does not polymerize A:U and U:A base pairs with these substrates, other Thg1 family enzymes have the ability to polymerize any of the four WC base pairs.[13] Although an in vivo function for 3′−5′ polymerization in yeast remains unknown, Thg1 family enzymes from every domain of life catalyze the WC-dependent reverse polymerase activity, suggesting that this may be an ancestral activity of the earliest Thg1 family members.[13,14] The 3′−5′ polymerase activity is likely exploited by TLPs to facilitate tRNA 5′ end repair and a 5′-tRNA editing reaction that occurs in the mitochondria of lower eukaryotes.[13,19] Despite the lack of identifiable sequence similarity between Thg1 and any other known enzyme, the putative active site of human Thg1 (hThg1) shares significant structural similarity with canonical WC-dependent 5′−3′ DNA/RNA polymerases. This suggests the possibility of a common evolutionary origin between 5′−3′ and 3′−5′ nucleotide addition enzymes.[20]

The long-term goal of this work is to determine the complete molecular mechanism for the unusual enzymatic activity catalyzed by Thg1. The hThg1 structure suggested that Thg1 utilizes two-metal ion catalysis, a feature also shared among canonical DNA/RNA nucleotidyl transferase enzymes,[21,22] and alanine-scanning mutagenesis previously identified 19 residues that are important for the overall G_{-1} addition reaction.[23] However, the precise roles of the metal ions and of individual Thg1 residues in the 3′−5′ addition reaction were not addressed by these earlier studies. To fully understand the complex, multistep reaction catalyzed by yThg1, we developed single-turnover kinetic assays that allow isolation and characterization of each of the three individual chemical steps that occur during addition of G_{-1} to $tRNA^{His}$ in yeast (adenylylation, nucleotidyl transfer, and pyrophosphate removal). Here we use this approach to construct a kinetic framework for the non-WC-dependent G_{-1} addition reaction catalyzed by yThg1, which is the first in-depth biochemical investigation into the molecular mechanism of any Thg1 family member. We also assign functional roles for nine highly conserved yThg1 residues that participate in the mechanism of G_{-1} addition.

MATERIALS AND METHODS

Nucleotides and Reagents. NTPs (100 mM LiCl salts) used for enzyme assays were purchased from Roche; [γ-^{32}P]ATP (6000 Ci/mmol), [α-^{32}P]ATP (3000 Ci/mmol), and [γ-^{32}P]GTP (6000 Ci/mmol) were purchased from Perkin-Elmer. Oligonucleotides were purchased from Sigma, and enzymes for labeled tRNA substrate preparation (T4 polynucleotide kinase and alkaline phosphatase) were from New England Biolabs. For Thg1 transient kinetic assays, ribonuclease A was purchased from Ambion and calf alkaline intestinal phosphatase from Invitrogen.

Thg1 Expression and Purification. *E. coli* strain BL21-DE3(pLysS) was used for overexpression and purification of yThg1, which was performed essentially as previously described for the N-terminally His_6-tagged enzyme.[14,23] Briefly, Thg1 proteins (wild-type and variants) were purified from a 0.5 L culture using immobilized metal ion affinity chromatography, dialyzed into buffer containing 50% glycerol for storage at −20 °C, and assessed for purity (≥90% for the wild type and all alanine yThg1 variants as judged by visual inspection of the purified enzyme preparation) using sodium dodecyl sulfate−polyacrylamide gel electrophoresis. Concentrations of wild-type and variant proteins were determined with the Bio-Rad protein assay; we note that the concentrations used for the kinetic measurements reflect the total concentration of Thg1 monomer in each reaction and are not adjusted for the fraction of active enzyme in each preparation.

Adenylylation Assay. Kinetic parameters for the adenylylation step of the G_{-1} addition reaction were determined at room temperature by reacting 5′-monophosphorylated [^{32}P]-$tRNA^{His}$ (p*$tRNA^{His}$) substrate (≤40 nM) with ATP in the presence of excess enzyme. The 5′-labeled [^{32}P]$tRNA^{His}$ was generated by in vitro transcription followed by phosphatase

dx.doi.org/10.1021/bi201397f | *Biochemistry* 2012, 51, 453−465

treatment and labeling with T4 polynucleotide kinase, as previously described.[16] Thg1 reaction buffer (used for all assays) contained 10 mM $MgCl_2$, 3 mM dithiothreitol (DTT), 125 mM NaCl, and 0.2 mg/mL BSA, buffered using either 25 mM 4-(2-hydroxyethyl)-1-piperazineethanesulfonic acid (HEPES) (pH 7.5) or a tribuffer system that spans a broad pH range {25 mM sodium acetate, 50 mM 2-[bis(2-hydroxyethyl)amino]-2-(hydroxymethyl)propane-1,3-diol (Bis-Tris), and 50 mM 2-amino-2-(hydroxymethyl)propane-1,3-diol-HCl (Tris)} for assays at pH 6.0.

For the determination of $K_{D,app}$tRNA, reactions were performed in the presence of a saturating concentration of ATP (1 mM) with varying concentrations of enzyme (0.05−15 μM) and were initiated by addition of enzyme to preincubated tRNA and ATP. For the determination of $K_{D,app}$ATP, reaction mixtures contained saturating concentrations of enzyme (15 μM) and varied ATP concentrations (0.1−3 mM), and the reactions were initiated by addition of ATP to preincubated enzyme and tRNA. At specific time points, a 5 μL aliquot was removed from each reaction mixture and placed in a new tube containing 0.5 μL of 500 mM ethylenediaminetetraacetic acid (EDTA) to quench the reactions and 0.5 μL of 10 mg/mL ribonuclease A (RNase A) to digest the labeled RNA preferentially after each pyrimidine, yielding a labeled 5′-oligonucleotide derived from the cleavage at nucleotide C_{+2}. The quenched reaction mixtures were incubated at 50 °C for 10 min, after which time, 0.5 unit of alkaline phosphatase was added to each quenched reaction mixture and incubated at 37 °C for 35 min to remove terminal phosphates from the digested reaction products. The resulting oligonucleotide App*GpC (corresponding to the adenylylated tRNA reaction product) and inorganic phosphate (P_i*, generated from unreacted tRNA) were resolved using silica TLC plates (EM Science) in an *n*-propanol/NH_4OH/H_2O (55:35:10, v:v:v) solvent system, visualized, and quantified using a Typhoon trio and ImageQuant (GE Healthsciences). A small amount of Ap*GpC oligonucleotide corresponding to addition of A_{-1} to the tRNA is also observed under these conditions; thus, the amounts of both products (App*GpC and A_{-1}p*GpC) were included for the determination of k_{obs}.

Time courses of product formation were plotted and fit to a single-exponential rate equation (eq 1) using Kaleidagraph (Synergy Software)

$$P_t = \Delta P[1 - \exp(-k_{obs}t)] \quad (1)$$

where P_t is the fraction of product formed at each time and ΔP is the maximal amount of product conversion observed during each time course.

The resulting k_{obs} values determined for each concentration of ATP or Thg1 were plotted and fit to eq 2 or eq 3, respectively, as described in the text to yield the pseudo-first-order maximal rate constants and dissociation constants. All reported kinetic parameters were determined using k_{obs} values derived from at least two independent experiments, and reported errors in k_{max} and $K_{D,app}$ are the least-squares estimates of the standard error derived from the fit to the data using Kaleidagraph.

$$k_{obs} = k_{max}[NTP]/(K_{D,app}NTP + [NTP]) \quad (2)$$

$$k_{obs} = k_{max}[Thg1]/(K_{D,app}tRNA + [Thg1]) \quad (3)$$

For yThg1 alanine variants with slow activity (<20% conversion to products after reaction for 4 h), k_{obs} was estimated using the method of initial rates, according to eq 4

$$k_{obs} = v_o/\Delta P \quad (4)$$

where v_o is the linear initial rate derived from the slope of the fraction of product versus time plots and ΔP is the maximal fraction of product conversion determined separately using wild-type Thg1 and the relevant substrate.

Nucleotidyl Transfer Assays. Kinetic parameters for the nucleotidyl transfer step were determined at room temperature by reacting a 5′-triphosphorylated [γ-^{32}P]$tRNA^{His}$ (5′p*pp-$tRNA^{His}$) substrate (100−300 nM) generated by in vitro transcription[16] with GTP in the presence of excess enzyme, in the Thg1 reaction buffers described above. At various time points, aliquots (3 μL) were removed and placed in a new tube containing 1 μL of 250 mM EDTA to quench the reactions, and then 2 μL of each quenched reaction mixture time point was spotted on PEI-cellulose TLC plates (EM Science). Plates were washed in 100% methanol, air-dried, and resolved using a 0.5 M potassium phosphate (pH 6.3)/methanol (80:20, v:v) solvent system to separate the labeled pyrophosphate ($P*P_i$) from unreacted labeled tRNA. For the determination of $K_{D,app}$GTP, the reaction mixtures contained a saturating concentration of enzyme (15 μM) preincubated with labeled tRNA, and reactions were initiated by the addition of varied concentrations of GTP (0.4−500 μM). For the determination of $K_{D,app}$tRNA, observed rates of nucleotidyl transfer were measured in reaction mixtures containing preincubated labeled tRNA and a saturating concentration of GTP (250 μM), and reactions were initiated by the addition of varied concentrations of the enzyme (0.5−30 μM). The k_{obs} for each condition was determined either by a fit of the time courses of product formation to the single-exponential rate equation (eq 1) or by the method of linear initial rates for slow reactions (eq 4) and further used to determine k_{ntrans} and K_D values (eqs 2 and 3), as described above for adenylylation.

Pulse Chase Nucleotidyl Transfer Assays. To generate labeled adenylylated $tRNA^{His}$, unlabeled p-$tRNA^{His}$ (0.5 μM) was incubated in a 36 μL reaction mixture containing 1−1.5 μCi (100−200 nM) of [α-^{32}P]ATP and excess yThg1 (15 μM) in Thg1 reaction buffer at room temperature for 1 h at pH 6.0 or for 3−4 h at pH 7.5. For each reaction, a chase was performed by addition of a large excess concentration of ATP and GTP, yielding a total reaction volume of 39 μL. For pH 6.0 reactions, the chased reaction mixtures contained final concentrations of 50 μM ATP and 250 μM GTP, and for pH 7.5 reactions, the final concentrations were 1.0 μM ATP and 25 μM GTP. At various times following the addition of the unlabeled GTP and ATP, aliquots of the reaction mixture (3 μL) were removed and placed in a new tube containing 1 μL of 250 mM EDTA to quench the reaction. An equal volume of sample loading dye (containing 95% formamide, 0.1% xylene cyanol, and 0.1% bromophenol blue) was added to each quenched reaction mixture, and products were resolved on a 10% polyacrylamide−4 M urea denaturing gel. The dried gel was visualized using a Typhoon trio (GE Healthsciences), and the amount of labeled tRNA at each time was quantified using ImageQuant (GE Healthsciences). Time courses of decay of the activated intermediate, normalized to the amount of activated tRNA present at the time of the chase, were fit either to eq 1 to yield k_{obs} (pH 7.5 data) or to both eqs 1 and 5 for the data at pH 6.0, where the double-exponential rate equation fits

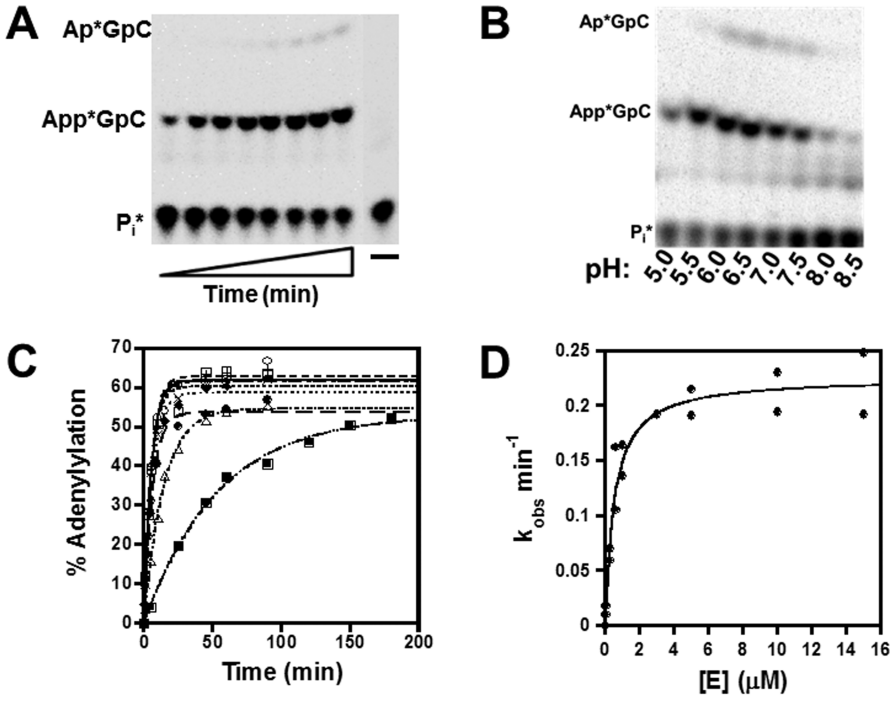

Figure 2. Single-turnover measurement of adenylylation kinetics. (A) Representative single-turnover adenylylation reaction mixture containing 3 μM yThg1, 1 mM ATP, and 5′-[^{32}P]tRNA^{His} (pH 6.0). Reaction products (AppGpC and ApGpC) were resolved from P_i generated from unreacted tRNA by silica TLC. (B) Adenylylation catalyzed by 5 μM yThg1 with 1 mM ATP at 1.5 h at the indicated pH (measured in the tribuffer Thg1 reaction system to span entire pH range). (C) Single-turnover adenylylation enzyme titration reactions were conducted at pH 6 with 1 mM ATP and 5′-[^{32}P]tRNA^{His} in the presence of 0.05 (■), 0.25 (△),0.6 (●), 1 (◆), 3 (×), 5 (+), 10 (□), and 15 μM yThg1 (○). Observed rates (k_{obs}) were determined by a fit to eq 1. (D) Observed rates of adenylylation were plotted as a function of [E] and fit to eq 3 to determine the first-order adenylation rate constant (k_{aden}) and apparent equilibrium dissociation constant (K_D) for ptRNA^{His}.

the data.

$$P_t = \Delta P_f[1 - \exp(-k_{obs-fast}t)] + \Delta P_s[1 - \exp(-k_{obs-slow}t)] \quad (5)$$

where ΔP_f is the amplitude of decay products that result from the fast-reacting state, ΔP_s is the amplitude of decay products resulting from the slow-reacting state, and $k_{obs-fast}$ and $k_{obs-slow}$ are the rate constants for the respective reactions.

Pyrophosphate Removal Assays. Kinetic parameters for removal of pyrophosphate were determined at room temperature by reacting a 5′-triphosphorylated [γ-^{32}P]G_{-1}-tRNA^{His} (5′p*pp G_{-1}tRNA^{His}) transcript (100−300 nM) in the presence of excess enzyme in the same reaction buffers described above. Observed rates (k_{obs}) for pyrophosphate removal were measured at varied concentrations of enzyme in the presence and absence of 1 mM GTP. Reactions were initiated by addition of enzyme to tRNA (with or without GTP), and 3 μL aliquots were quenched at various time points by addition of 1 μL of 250 mM EDTA. The removal of pyrophosphate (P*P_i) from unreacted tRNA was visualized using PEI-cellulose TLC, as described above for nucleotidyl transfer. Time courses of product formation for wild-type Thg1 were fit to eq 1 to yield k_{obs}. For alanine variants with low activity (time courses indicate linear product formation after 4 h), k_{obs} was estimated using the method of initial rates (eq 4). Pseudo-first-order maximal rate constants and dissociation constants were determined using eq 3.

Preparation and Analysis of yThg1 Alanine Variants. yThg1 alanine variants R27A, D29A, D77A, E78A, K44A, N161A, R133A, and K96A were described previously.[20,23] The S76A yThg1 variant was created for this study using QuikChange (Agilent) according to the manufacturer's instructions, using complementary pairs of oligonucleotides and the plasmid encoding N-terminally His_6-tagged yeast Thg1 as the template for the mutagenesis experiment. Thg1 variant proteins were purified using immobilized metal ion affinity chromatography as described above for wild-type yThg1. The kinetic parameters for adenylylation of nucleotidyl transfer were measured at the optimal pH for each activity determined with the wild-type enzyme, using each alanine variant (15 μM) under single-turnover conditions. Reactions with higher concentrations of Thg1 to test for saturation of the observed rates with respect to tRNA were conducted for certain variants, as indicated in the text. For adenylylation, reactions were performed at pH 6.0 and mixtures contained varied concentrations of ATP (0.075−5 mM); nucleotidyl transfer reactions were performed at pH 7.5, and mixtures contained varied concentrations of GTP (0.005−2 mM). Observed rates for each concentration of NTP were determined using eq 1 or by the method of initial rates (eq 4) for variants with slow catalytic activity and fit to eq 2 to yield the k_{max} and $K_{D,app}$NTP for the indicated step. For pyrophosphate removal, a single k_{obs} measurement was performed with each variant enzyme (15 μM) at pH 7.5; reported values are the average of at least two independent experiments.

RESULTS

Analysis of the Activation Step. Using single-turnover conditions ([E]/[tRNA] ≥ 5), we measured the observed rate (k_{obs}) for each of the three chemical steps for the nontemplated addition of G_{-1} to yeast tRNA^{His}, and the dependence of those

Table 1. Kinetic Parameters for Addition of G_{-1} to $tRNA^{His}$ Catalyzed by Yeast Thg1

	pH 6			
	k_{max} (min^{-1})	$K_{D,app}$tRNA (μM)	k_{max} (min^{-1})	$K_{D,app}$NTP (μM)
adenylylation	0.23 ± 0.01	0.51 ± 0.09	0.45 ± 0.03	360 ± 80
nucleotidyl transfer	0.20 ± 0.01	1.3 ± 0.3	0.24 ± 0.01	16 ± 2
pp removal with GTP	0.15 ± 0.01	0.4 ± 0.1	N/A	N/A
pp removal without GTP	0.002−0.003[a]	<5[b]	N/A	N/A
	pH 7.5			
	k_{max} (min^{-1})	$K_{D,app}$tRNA (μM)	k_{max} (min^{-1})	$K_{D,app}$NTP (μM)
adenylylation	>0.06[c]	>15[d]	ND[e]	ND[e]
nucleotidyl transfer	3.6 ± 0.3	7 ± 2	3.0 ± 0.1	21 ± 4
pp removal with GTP	0.77 ± 0.04	2.5 ± 0.4	N/A	N/A
pp removal without GTP	0.030 ± 0.003	1.6 ± 0.7	N/A	N/A

[a]Estimated on the basis of values for k_{obs} at the highest concentrations of enzyme tested (5−15 μM). [b]Upper limit for K_DtRNA, based on saturation of k_{obs} measured in assays with ≥5 μM yThg1. [c]Lower limit at pH 7.5 based on the k_{obs} for adenylylation at the highest concentration of enzyme achievable in the assays [15 μM (see Figure S1B of the Supporting Information)]. [d]Lower limit for K_DtRNA based on the highest concentration of enzyme achievable in the assays. [e]Not determined.

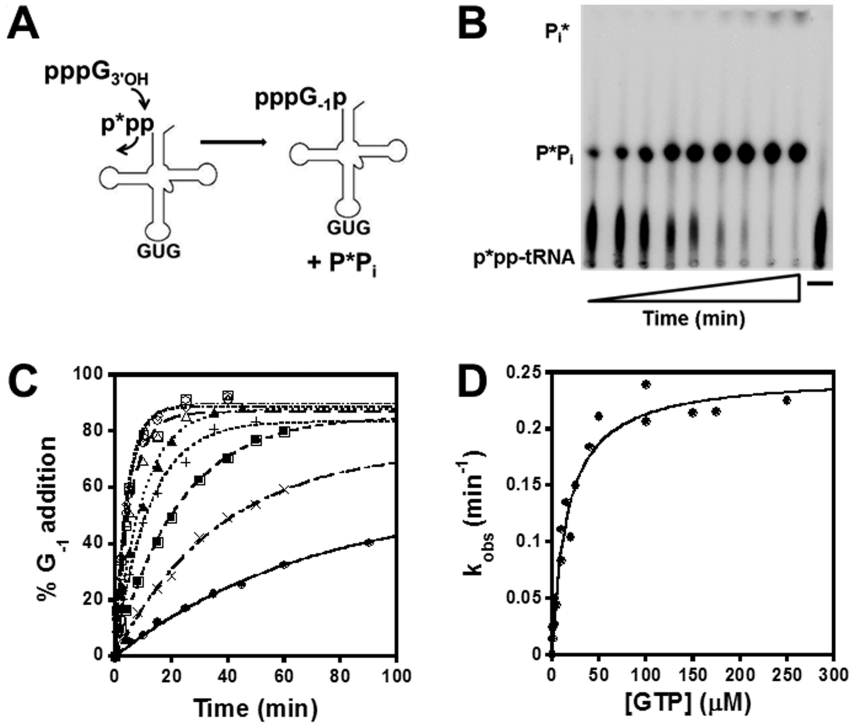

Figure 3. Single-turnover measurement of nucleotidyl transfer with ppptRNA^{His}. (A) Nucleotidyl transfer assay scheme with 5′-ppp-tRNA^{His} labeled at the γ-phosphate. Addition of G_{-1} results in the release of labeled PP_i. (B) Representative single-turnover nucleotidyl transfer assay containing 250 μM GTP, 15 μM yThg1, and 5′-ppp-tRNA^{His} at pH 6, resolved by PEI-cellulose TLC. (C) Single-turnover nucleotidyl transfer GTP titration reaction at pH 6, conducted with a saturating level of yThg1 (15 μM) in the presence of 1 (◆), 3 (■), 5 (▲), 10 (×), 20 (+), 40 (△), 100 (●), 150 (□), and 175 μM GTP (◇). Observed rates (k_{obs}) were determined by a fit to eq 1. (D) Observed rates of nucleotidyl transfer plotted as a function of GTP concentration and fit to eq 2 to determine the first-order nucleotidyl transfer rate constant (k_{ntrans}) and apparent equilibrium dissociation constant (K_D) for GTP.

rates on concentration of enzyme or nucleotide, as appropriate for the step being investigated. To characterize adenylylation, we used an assay that measures protection of a labeled tRNA 5′-phosphate from removal by alkaline phosphatase, due to reaction at the 5′ end of the tRNA. After incubation of a 5′-monophosphorylated [^{32}P]tRNA^{His} (p*tRNA^{His}) substrate (≤40 nM) with ATP in the presence of excess yThg1, the amount of adenylylated tRNA (visualized as App*GpC) was quantified as a function of time (Figure 2A). A slow rate of addition of A_{-1} to the adenylylated tRNA was observed in the absence of the preferred GTP substrate for G_{-1} addition. The amount of this product (visualized as A_{-1}p*GpC) was included in the total amount of adenylylated reaction product.

Time courses of product formation fit well to a single-exponential equation (eq 1) (Figure S1A of the Supporting Information) and were not dependent on the order of mixing reactants or the concentration of tRNA tested (data not shown). No lags in product formation were observed at any concentrations of the enzyme or nucleotide cofactors tested, suggesting a rapid equilibrium mechanism, in which the initial binding of enzyme and substrate is rapid and dissociation of substrate is faster than the maximal k_{aden} ($k_{off} \gg k_{aden}$).[24,25]

dx.doi.org/10.1021/bi201397f | Biochemistry 2012, 51, 453−465

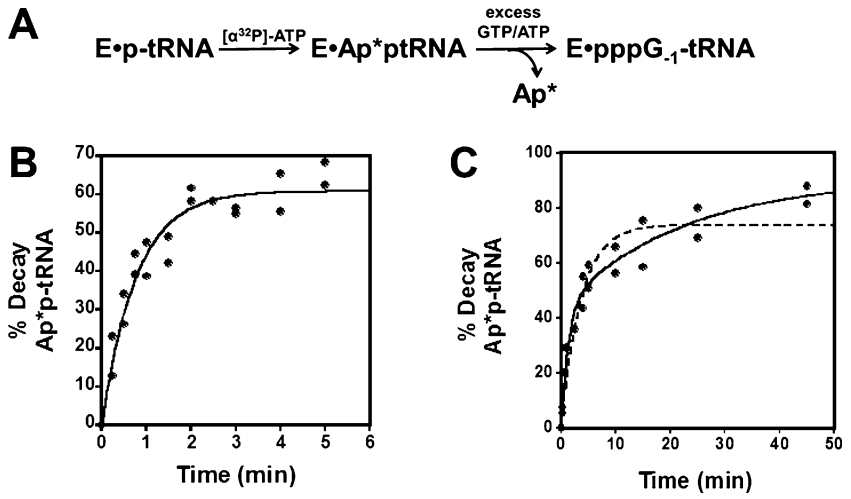

Figure 4. Rate of nucleotidyl transfer of G_{-1} to adenylylated tRNA. (A) Pulse chase reaction scheme. Formation of 5′-adenylylated $tRNA^{His}$ labeled at the α-phosphate of AMP is followed by addition of unlabeled GTP (substrate for nucleotidyl transfer) as well as excess unlabeled ATP to trap any remaining unreacted tRNA. The decay of radiolabeled tRNA corresponds to the rate of addition of G_{-1} to the adenylylated tRNA. (B) Observed rate of nucleotidyl transfer for the reaction chased with 25 μM GTP and 50 μM ATP at pH 7.5 determined by a fit to eq 1. (C) Observed rate of nucleotidyl transfer for the reaction chased with 250 μM GTP and 50 μM ATP at pH 6. Both single-exponential (eq 1; $R^2 = 0.93$; dashed line) and double-exponential (eq 5; $R^2 = 0.97$; solid line) fits to the data are shown.

Thus, the dependence of k_{obs} on the varied reactant (NTP or enzyme) reveals the apparent binding constant for NTP or tRNA, respectively, and the pseudo-first-order maximal rate constant for each reaction (according to eqs 2 and 3). Saturating concentrations of the nonvaried reactant were included in each assay. For each of the steps, the observed maximal rate constant (k_{aden}, k_{ntrans}, or k_{ppase}) may reflect the rate of the actual chemical step or of a rate-determining conformational change that precedes chemistry. Identification of the precise nature of the rate-determining step requires further characterization.

At pH 7.5, the same pH used previously for determination of steady-state kinetic parameters for yThg1-catalyzed G_{-1} addition,[18] observed rates of adenylylation did not saturate but remained linearly dependent on yThg1 concentration even at the highest concentration of enzyme that could be achieved in the assay, providing a lower limit to k_{aden} and $K_{D,app}$tRNA at pH 7.5 (Figure S1B of the Supporting Information and Table 1). To address this limitation, we investigated the extent of adenylylation after 1.5 h in the pH range of 5.0−8.5, revealing a maximal amount of adenylylated product formed at pH 6.0 (Figure 2B). At pH 6.0, observed rates of adenylylation exhibit the expected hyperbolic dependence on both enzyme and ATP concentration, and $K_{D,app}$ and k_{aden} were determined at this pH (Figure 2, Figure S2 of the Supporting Information, and Table 1). For both enzyme and ATP titration experiments, the measured k_{aden} values were in reasonable agreement (0.23 ± 0.01 and 0.45 ± 0.03 min^{-1}, respectively).

Single-Turnover Measurement of Nucleotidyl Transfer. Kinetic parameters for the second step, nucleotidyl transfer, were determined by reacting a 5′-triphosphorylated [γ-^{32}P]$tRNA^{His}$ (p*pp-$tRNA^{His}$) substrate with GTP and enzyme and quantifying the release of labeled PP_i following G_{-1} addition (Figure 3). The faster steady-state k_{cat} previously measured for reaction with ppp-$tRNA^{His}$ compared with the k_{cat} for p-$tRNA^{His}$[16] suggests that the ppp-$tRNA^{His}$ substrate is kinetically competent to mimic the nucleotidyl transfer step that occurs with App-$tRNA^{His}$ during the physiological G_{-1} addition reaction (see Figure 1), which we also confirm below. All reaction mixtures contained limiting tRNA and saturating amounts of the nonvaried reactant (250 μM GTP for enzyme titration and 15 μM yThg1 for GTP titration). As with adenylylation, time courses were well fit by the single-exponential equation, no lags in product formation were observed, and k_{obs} did not depend on the order of mixing or the concentration of tRNA (Figure 3C and data not shown). Rates of nucleotidyl transfer (k_{obs}) were measured at pH 6.0 and 7.5. In contrast to the adenylylation step, hyperbolic reaction kinetics were observed with respect to GTP (Figure 3D and Figure S3 of the Supporting Information) and enzyme (data not shown) at both pH values, allowing for determination of pseudo-first-order maximal rate constants (k_{ntrans}) and apparent dissociation constants ($K_{D,app}$GTP and $K_{D,app}$tRNA) (Table 1). k_{ntrans} was 10-fold faster at pH 7.5 (3.0 ± 0.1 min^{-1}) than at pH 6.0 (0.24 ± 0.01 min^{-1}) (Table 1). Similar k_{ntrans} values were also obtained regardless of whether enzyme or GTP was varied in the assay (Table 1).

To further investigate the kinetic competence of ppp-$tRNA^{His}$ as a mimic of the adenylylated tRNA intermediate, a pulse chase experiment was performed to directly measure the rate of addition of nucleotide to App-$tRNA^{His}$. In this experiment, unlabeled $ptRNA^{His}$ was incubated with [α-^{32}P]ATP and excess yThg1 (15 μM), yielding Ap*p-$tRNA^{His}$ with a label in the AMP moiety (Figure 4A). A sufficient amount of time was allowed for accumulation of maximal amounts of adenylylated tRNA, based on previous time courses. At this point ($t = 0$), a large excess of unlabeled ATP and GTP was added to the reaction mixtures. Reaction of GTP with the labeled Ap*ptRNA causes displacement, and hence loss of the radiolabel from the tRNA, while the ATP trapped any remaining unreacted p-$tRNA^{His}$, ensuring only preformed labeled Ap*$ptRNA^{His}$ present at the time of the chase was observed in the assay. Time courses of loss of the radiolabel from the intermediate, normalized to the amount of activated tRNA present at the time of the chase, were plotted and fit to a single- or double-exponential rate equation.

At pH 7.5, data for reactions chased with 25 μM GTP were fit well by a single-exponential equation (eq 1), yielding a k_{obs}

dx.doi.org/10.1021/bi201397f | Biochemistry 2012, 51, 453−465

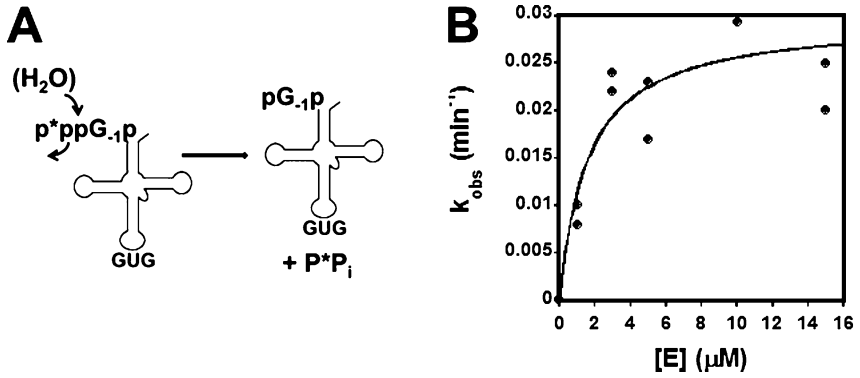

Figure 5. Rate of removal of pyrophosphate from the G_{-1}-containing tRNA. (A) Reaction scheme for the assay of diphosphatase activity using γ-^{32}P-labeled $pppG_{-1}$-$tRNA^{His}$. Removal of labeled PP_i is measured using PEI-cellulose TLC. (B) Single-turnover measurement of k_{ppase} and $K_{D,app}$tRNA at pH 7.5, determined by a fit of the data to eq 3.

of 1.3 ± 0.1 min^{-1} (Figure 4B), in close agreement with the k_{obs} (1.1 min^{-1}) measured at the same concentration of GTP with the ppp-$tRNA^{His}$ substrate (Figure S3 of the Supporting Information). At pH 6.0, data for reactions chased with 250 μM GTP can be fit with either single-exponential (k_{obs} = 0.28 ± 0.04 min^{-1}) or double-exponential ($k_{obs-fast}$ = 0.78 ± 0.25 min^{-1}, and $k_{obs-slow}$ = 0.044 ± 0.029 min^{-1}) equations (eq 5), with approximately equal amplitudes (45%) for each phase of the reaction (Figure 4C). Although the R^2 value for the fit to the double-exponential equation (0.97) is higher than for the fit to the single-exponential equation (0.93), the larger uncertainty in the rate constants derived from the double-exponential fit makes it difficult to assess which fit better describes the observed data; thus, both are shown. Observation of the double-exponential behavior would suggest that at pH 6.0 there are two states, not in equilibrium with each other, which react with different rates. These data could be explained by a slow conformational change in the ES complex, followed by a fast step leading to formation of products, or two conformations of enzyme that react with differing rates to generate products; further experimental evidence is required to distinguish these possibilities. Nonetheless, whether the data reflect a single rate of reaction, or two, the rate of addition of nucleotide to App-$tRNA^{His}$ is still within reasonable agreement with the k_{obs} of 0.21 min^{-1} measured at 250 μM GTP with the ppp-$tRNA^{His}$ substrate (Figure 3D). These data suggest that addition to ppp-$tRNA^{His}$ occurs by the same mechanism as addition to the adenylylated tRNA, and thus, kinetic parameters obtained with ppp-$tRNA^{His}$ are likely to reflect the same rate-determining step for the nucleotidyl transfer reaction, regardless of the identity of the activating group on the 5′ end of the tRNA substrate.

Pyrophosphate Removal Is Stimulated by the Addition of GTP. Kinetic parameters for the third step of G_{-1} addition, removal of pyrophosphate, were determined using a 5′-triphosphorylated [γ-^{32}P]p*ppG_{-1}-containing $tRNA^{His}$ transcript that mimics the product of the nucleotidyl transfer step formed by yThg1 (Figure 5A). Reactions were performed under single-turnover conditions with limiting tRNA, and the release of labeled pyrophosphate was observed as previously described. Time courses of pyrophosphate release were fit to a single-exponential equation (eq 1) to yield k_{obs}, with no detectable lags in product formation at any concentration of yThg1 (data not shown). Saturation kinetics were observed at pH 7.5, and the pseudo-first-order maximal rate constant (k_{ppase}) and $K_{D,app}$tRNA were determined using eq 2 (Table 1). Although the observed rates of pyrophosphate removal measured at pH 6 did not change significantly between 5 and 15 μM enzyme (k_{obs} = 0.002−0.003 min^{-1}), these rates were too slow for determination of $K_{D,app}$tRNA (data not shown). Therefore, we estimate $K_{D,app}$tRNA (pH 6) to be <5 μM (Table 1).

The removal of pyrophosphate does not necessarily require participation of an NTP substrate (Figures 1 and 5A). However, in the presence of a saturating amount of enzyme and 1 mM GTP, the observed rates of pyrophosphate removal were measureably enhanced. k_{ppase} was stimulated 30-fold at pH 7.5 (k_{ppase} = 0.77 ± 0.04 min^{-1}) and 80-fold at pH 6.0 (k_{ppase} = 0.15 ± 0.01 min^{-1}) (Table 1). It is unlikely that the stimulation results from addition of further GTP nucleotides to $pppG_{-1}$-tRNA (to yield G_{-2}-containing tRNA), which would similarly cause release of labeled PP_i in reactions, because addition of G_{-2} does not occur at significant levels with the wild-type (A_{73}-containing) $tRNA^{His}$ used in these assays.[18] Similar amplitudes are observed (maximum of 80−85% PP_i released) for reactions in the presence and absence of nucleotide, suggesting that the increase in k_{ppase} is not attributable to −1 addition to significant amounts of aberrantly G_{+1}-initiated substrate that may have arisen during in vitro transcription. Previously reported steady-state kinetic parameters for the overall G_{-1} addition reaction were determined in the presence of similarly high concentrations of GTP,[16] suggesting that the k_{ppase} measured in the presence of GTP reflects the rate of this step during the multiple-turnover reaction.

Application of the Kinetic Framework in Identifying Catalytic Residues That Participate in G_{-1} Addition. yThg1 and human Thg1 (hThg1) share significant (69%) sequence similarity, including conservation of all 19 residues implicated as being important for G_{-1} addition activity in the earlier alanine-scanning mutagenesis.[23] Therefore, using the hThg1 crystal structure in conjunction with our kinetic framework for yThg1 activity, we investigated how highly conserved yThg1 residues are involved in the catalytic mechanism of G_{-1} addition. Despite the recent availability of a Thg1 structure, questions remain about the mechanism that are not fully addressed by the structural data, particularly because the current structure lacks bound tRNA (and thus any information about tRNA recognition). In addition, the involvement of multiple nucleotides in different ways for each step of the G_{-1} addition reaction makes it difficult to unambiguously assign identities to the bound nucleotides visualized in the structure. Finally, because the available structural data are for the hThg1 enzyme, while the kinetic

dx.doi.org/10.1021/bi201397f | Biochemistry 2012, 51, 453−465

analysis was performed with yThg1, the possibility that residues implicated by the structure in catalysis may not function similarly in the context of these two different, albeit highly homologous, enzymes must be addressed. Thus, the need for detailed kinetic investigation of the three steps of the G_{-1} addition reaction to test roles for residues predicted by the structure is clear.

Our kinetic analysis indicates that k_{ntrans} and k_{ppase} increase from pH 6.0 to 7.5 while k_{aden} decreases across this range (Table 1). These data imply that different ionization events may be important for the different chemical steps of the reaction, suggesting the possibility that independently functioning amino acid residues may be identified. Using the biochemical assays described previously, under optimal conditions for each step, we measured transient kinetic parameters for nine yThg1 alanine variants chosen because of their location near the bound nucleotides revealed by the crystal structure (R27A, D29A, K44A, S76A, D77A, E78A, K96A, R133A, and N161A) (Figure 6).[20] All of these yThg1

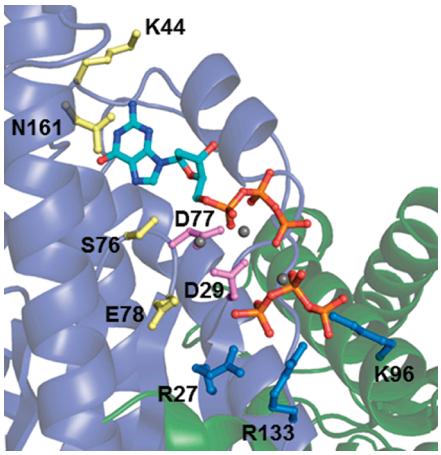

Figure 6. Catalytic residues in the human Thg1 active site. A view of the hThg1 active site containing two bound dGTP molecules (for the second bound dGTP, only the triphosphate moiety is visible in the electron density map),[20] with residues investigated in this study highlighted. The numbering is according to the yThg1 residue position. Each residue side chain is colored according to the kinetic effects observed here. Yellow residues are those with more significant defects in adenylylation kinetics (K44, S75, E78, and N161); blue residues are those with the most severe defects in nucleotidyl transfer kinetics (R27, K96, and R133). The two metal ion-binding carboxylates (D29 and D77) that are critical for all three chemical steps of the yThg1 reaction are highlighted in magenta.

variants with the exception of S76A were previously tested and shown to exhibit significant reductions in the overall specific activity of G_{-1} addition.[20,23] S76A was also chosen for further study because the analogous alteration in hThg1 (S75A) affected adenylylation during analysis of the hThg1 crystal structure.[20] Numbering of residues throughout is according to positions in the yeast sequence, with the equivalent residue in hThg1 indicated by parentheses, if different from the yeast residue numbering. Analysis of kinetic parameters for these variants in conjunction with the structural data has allowed us to assign functional roles for these highly conserved Thg1 residues.

Two-Metal Ion Catalysis May Be Used for All Three Chemical Steps of G_{-1} Addition. In the hThg1 crystal structure, D29 and D76(D77) coordinate two metal ions believed to be important for catalysis and are located in positions analogous to those of two highly conserved carboxylate residues (D475 and D654 in T7 DNA Pol) important for 5′−3′ addition by family A DNA polymerases.[20,26,27] The two aspartates are critical for the overall G_{-1} addition reaction, as indicated by the severe defects in specific activity upon alteration to alanine in either yeast or human Thg1.[20,23] Transient kinetic measurements revealed severe reductions in k_{obs} for all three chemical steps for the yThg1 D29A and D77A variant enzymes (Table 2). Between these two variants, the only step for which detectable rates could be measured was for nucleotidyl transfer catalyzed by D77A yThg1. Importantly, while the k_{ntrans} for the D77A variant was reduced by 30000-fold as compared to that of the wild type, $K_{D,app}$GTP was relatively unaffected (Table 2). These data strongly suggest that D76 and D77, and likely the two metal ions coordinated by these residues, participate in the rate-determining process for each of the three chemical steps of the 3′−5′ addition reaction catalyzed by yThg1. Moreover, at least for the D77A variant, the similar K_D for the GTP nucleotide suggests that the alteration has not significantly perturbed the global protein structure, and the kinetic effects of these changes reflect changes in catalytic activity, not structure, of the variant enzyme. Because of the undetectable rates of reaction exhibited in most assays with these variants even at enzyme concentrations that are saturating for the wild-type enzyme (15 μM), we note that potential tRNA binding defects could also contribute to the decreased catalysis observed upon alteration of the metal-binding carboxylates.

A third carboxylate, E78(E77), is located at a position in the structure analogous to the position of the highly conserved E655 in T7 DNA Pol.[20,27] In both hThg1 and T7 Pol, the glutamate side chain points away from the metals (Figure 6). As with E655 in T7 DNA Pol, alteration of E78(E77) to alanine causes only minor defects in catalysis in hThg1; however, the E78A alteration in yeast Thg1 causes severe defects in G_{-1} addition, both in vitro and in vivo in yeast.[20,23,28] From analysis of the three steps, the source of the E78A defect in yThg1 can be substantially attributed to the adenylylation step, which is affected by at least 4000-fold, as compared to the relatively moderate effects on the rates of nucleotidyl transfer and pyrophosphate removal (decreased 20- and 60-fold, respectively) (Table 2 and Figure 7). These data suggest a difference between the requirement for the third carboxylate residue between yeast and human Thg1 that is directly related to a difference in the adenylylation step of the reaction, which could include differences in the rate-determining step for chemistry or binding of tRNA or nucleotide substrates.

K44 and N161 Participate in the Adenylylation Step. Previously, we implicated S76(S75) of hThg1 in adenylylation and on this basis proposed that one of the bound nucleotides observed in the hThg1 structure mimics the position of the ATP used for activation of the tRNA. In the hThg1 structure, S76(S75) makes a direct contact with N_7 of the bound dGTP, and alteration of the serine to alanine in the human enzyme causes a 10-fold increase in $K_{D,app}$ATP.[20] As with hThg1, alteration of the analogous serine residue (S76) in yThg1 to alanine causes a significant defect in adenylylation, while the kinetics for nucleotidyl transfer and pyrophosphate removal remain relatively unchanged (Table 2). We identified two additional residues, K44 and N161, which, unlike S76(S75), are not observed to make direct contacts with the bound nucleotide base in the hThg1 structure but are located nearby

Table 2. Kinetic Parameters for G_{-1} Addition Catalyzed by Yeast Thg1 Alanine Variants[a]

	adenylylation			nucleotidyl transfer			ppase
	k_{aden} (min^{-1})	$K_{D,app}ATP$ (μM)	k_{aden}/K_D (μM^{-1} min^{-1})	k_{ntrans} (min^{-1})	$K_{D,app}GTP$ (μM)	k_{ntrans}/K_D (μM^{-1} min^{-1})	k_{obs} (min^{-1})
WT	0.45 ± 0.03	360 ± 80	(1.3 ± 0.3) × 10^{-3}	3.0 ± 0.2	25 ± 6	0.12 ± 0.03	0.027 ± 0.001
D29A	UD[b]	UD[b]	UD[b]	UD[b]	UD[b]	UD[b]	UD[b]
D77A	UD[b]	UD[b]	UD[b]	(1.1 ± 0.1) × 10^{-4}[c]	11 ± 4	(1.0 ± 0.4) × 10^{-5}	UD[b]
E78A	UD[b]	UD[b]	UD[b]	0.16 ± 0.02	216 ± 74	(7 ± 3) × 10^{-4}	(5.2 ± 0.2) × 10^{-4}[c]
K44A	(2.7 ± 0.5) × 10^{-3}[c]	4000 ± 1000	(7 ± 2) × 10^{-7}	0.45 ± 0.05	23 ± 9	0.020 ± 0.008	0.028 ± 0.003
N161A	(5.4 ± 0.6) × 10^{-3}[c]	1400 ± 400	(4 ± 1) × 10^{-6}	1.2 ± 0.1	34 ± 8	0.034 ± 0.008	0.009 ± 0.001
S76A	~0.03[d]	<3000[e]	>1 × 10^{-5}	1.0 ± 0.1	45 ± 12	0.023 ± 0.006	0.015 ± 0.001
R27A	(8.4 ± 0.7) × 10^{-4}[c]	300 ± 100	(3 ± 1) × 10^{-6}	(5.8 ± 0.4) × 10^{-4}[c]	230 ± 60	(2.5 ± 0.7) × 10^{-6}	0.016 ± 0.001
R133A	(1.8 ± 0.9) × 10^{-3}[c]	170 ± 40	(1.1 ± 0.6) × 10^{-5}	(3.8 ± 0.3) × 10^{-4}[c]	85 ± 30	(4.5 ± 2) × 10^{-6}	0.025 ± 0.001
K96A	(2.3 ± 0.9) × 10^{-3}[c]	320 ± 50	(7.2 ± 3) × 10^{-6}	(8.6 ± 0.7) × 10^{-3}[c]	240 ± 70	(4 ± 1) × 10^{-5}	0.016 ± 0.001

[a]Kinetic parameters for alanine variants were measured at optimal pH values for each step of the G_{-1} addition reaction in the presence of a saturating concentration of enzyme (15 μM) with respect to wild-type yeast Thg1. Adenylylation reactions were at pH 6 in the presence of varied ATP concentrations (0.075−5 mM). Nucleotidyl transfer reactions were conducted at pH 7.5 in the presence of varied GTP concentrations (0.005−2 mM). Time courses of pyrophosphate removal were determined at pH 7.5 in the absence of GTP, and the reported k_{obs} values are the average of two independent measurements. [b]Product formation was not detected above background after 4 h. [c]k_{max} values derived from observed rates determined using the method of initial rates. [d]Estimate for k_{aden} based on a similar k_{obs} measured in reactions with ≥3 mM ATP. [e]Upper limit to K_DATP determined from the lowest ATP concentration that yielded the maximal k_{obs} for the reaction.

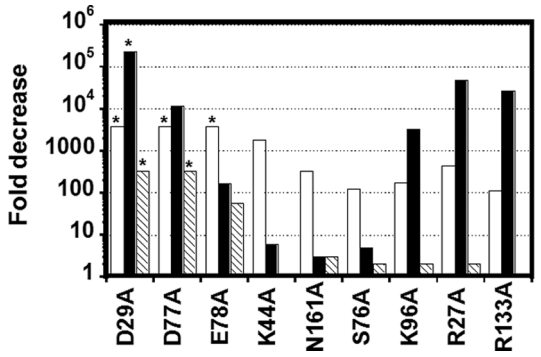

Figure 7. Effects on adenylylation, nucleotidyl transfer, and pyrophosphate removal caused by yThg1 alanine alterations. For each variant, the fold decrease in activity was calculated by determining the ratio of the measured activities of the wild type to that of the indicated yThg1 variant enzyme. For adenylylation (white bars) and nucleotidyl transfer (black bars), the indicated value is the fold decrease in the overall catalytic efficiency, as reflected by the $(k_{max}/K_{D,app}NTP^{WT})/(k_{max}/K_{D,app}NTP^{mut})$ measured for each step under the conditions defined in Table 2. For pyrophosphate removal (hatched bars), the fold decrease caused by the alanine alteration was determined by the comparison of k_{obs} for the wild type vs each variant, measured with 15 μM yThg1 at pH 7.5. Values denoted with asterisks represent the lower limit to the fold decrease calculated for variants that exhibit undetectable levels of activity under the conditions of the assay.

(Figure 6). K44 resides on a loop ~5 Å from the bound nucleotide, and N161 is located on an α-helical region ~8 Å from the nucleotide. The measured catalytic efficiencies for the adenylylation step, as reflected by $k_{aden}/K_{D,app}ATP$, for K44A and N161A are reduced by 2000- and 300-fold, respectively, while $k_{ntrans}/K_{D,app}GTP$ and k_{obs} for pyrophosphate removal are only modestly affected (<10-fold) compared to those of the wild type (Table 2 and Figure 6). To ensure that defects in tRNA binding are not responsible for the substantial decrease in the maximal rate constant for adenylylation, we measured k_{obs} for each variant with saturating ATP concentrations at several high concentrations of Thg1 (15−30 μM). At all concentrations, the measured rates did not vary significantly, indicating that $K_{D,app}$tRNA is not substantially affected by these alterations (data not shown). Moreover, for each of these variants, the relatively unaffected rate of pyrophosphate removal suggests that the overall protein fold remains intact in each variant, and as described above, the observed kinetic effects reflect changes in groups that actively participate in catalysis.

The yThg1 S76A variant displayed distinct kinetic behavior for the adenylylation step. In time courses, k_{obs} did not change significantly between 0.075 and 5 mM ATP (the measured k_{obs} varied between 0.02 and 0.03 min^{-1}). However, in the lower part of this ATP concentration range (0.075−3 mM), the amplitude of total reaction products increased from 7 to 63%, until maximal product amplitudes (62−63%) were reached for ATP concentrations of >3 mM (Figure S4A of the Supporting Information). Amplitudes of reaction products in nucleotidyl transfer experiments for S76A yThg1 reached the same maximal values at all GTP concentrations tested, and the catalytic efficiency for this step ($k_{ntrans}/K_{D,app}GTP$) was reduced by only 5-fold (Figure S4B of the Supporting Information and Table 2). Therefore, these kinetic effects are specific to adenylylation. Because the amplitude of the single-turnover time course reflects the amount of convertible tRNA substrate in each reaction mixture, a likely interpretation of these data is that, at low ATP concentrations, the lack of the S76 hydroxyl-containing side chain promotes an alternative catalytically inactive conformation of tRNA-bound enzyme to accumulate, and sufficiently high ATP concentrations are needed to overcome the inactive conformation. These data provide further evidence that different modes of nucleotide binding occur within the Thg1 active site and can affect the reactivity of the enzyme, also consistent with the unexpected role we observed for GTP in stimulating removal of pyrophosphate (Table 1).

A Second Bound Nucleotide Appears To Represent the Position of the Incoming GTP for Nucleotidyl Transfer. For yThg1 variants R27A, K96A, and R133A, there is a 100−450-fold reduction in the overall catalytic efficiency for adenylylation (as represented by $k_{aden}/K_{D,app}ATP$) (Table 2 and Figure 7). However, the catalytic efficiency of

nucleotidyl transfer is reduced much more substantially, with $k_{ntrans}/K_{D,app}$for GTP decreased by 3000−50000-fold (Figure 7). As with the adenylylation defective variants described above (K44A, N161A, and S76A), the observed rate of pyrophosphate removal is minimally affected by these alterations, suggesting that the global enzyme fold is not altered significantly by the alterations (Table 2).

Because these highly conserved lysine and arginine residues could potentially interact with negatively charged backbone residues of the $tRNA^{His}$ substrate, we tested whether defects in tRNA binding caused by these alterations may contribute to the observed decreases in the rates of adenylylation or nucleotidyl transfer. Although the slow rates make it difficult to directly measure K_D values for tRNA, we tested whether the observed maximal rate constants were saturating for tRNA by measuring the k_{obs} for each reaction at several high concentrations of Thg1 (10−20 μM) and saturating concentrations of NTP. For the R133A variant, observed maximal rates of adenylylation and nucleotidyl transfer did not depend on the concentration of Thg1 at ≥15 μM enzyme in the assays, suggesting that $K_{D,app}$tRNA is not substantially altered from that of the wild type with this variant (data not shown). For R27A, the rate of adenylylation is similarly insensitive to changes in enzyme concentration, but the k_{obs} for nucleotidyl transfer increases across this concentration range, suggesting that saturation for tRNA binding has been achieved for adenylylation, but potentially not for nucleotidyl transfer (data not shown). While there may be some defect in tRNA binding associated with the R27A alteration, the fact that this defect is specific to only the nucleotidyl transfer step (and not adenylylation or pyrophosphate removal) argues that the alteration does not cause a global change in tRNA recognition or binding and reinforces our observation that this residue exerts its primary function during nucleotidyl transfer. For the K96A alteration, k_{obs} values for both adenylylation and nucleotidyl transfer increase across the 10−20 μM concentration range tested, suggesting that defects in tRNA binding may contribute significantly to the decreased catalytic efficiencies measured for this variant. Again, the relatively unaffected rate of pyrophosphate removal indicates that tRNA binding is not generally defective with the K96A variant. Further investigations of tRNA binding will be required to address these possibilities directly. We note that although adenylylation is certainly less efficiently catalyzed by all three variants, the decreases are entirely attributed to a decrease in the rate-determining step for chemistry (which may include changes in the positioning of the tRNA substrate that affect reactivity), with little change in the binding affinity for the activating ATP (Table 2).

Taken together, these data reveal that R27, K96, and R133 play a major role in nucleotidyl transfer. The decrease in catalytic efficiency for nucleotidyl transfer is driven by both a substantial decrease in k_{ntrans} and a 3−10-fold increase in $K_{D,app}$GTP, suggesting that these residues play important roles both in binding the GTP to be added in the 3′−5′ addition reaction and in the rate-determining step for chemistry, which may include the positioning of the tRNA substrate for catalysis. In the hThg1 crystal structure, R27, K96(K95), and R133-(R131) make direct contacts with the triphosphate of a second bound dGTP in the Thg1 active site (Figure 6).[20] The position of the base and sugar of the second dGTP cannot be determined because of the lack of density observed for the rest of this nucleotide in the hThg1 structure, and therefore, the orientation of the 3′-OH that would act as the nucleophile for the 3′−5′ addition step, relative to the metal ions, remains to be determined. Nevertheless, our kinetic data suggest that the triphosphate moiety captured in the hThg1 structure may represent the position of the incoming GTP used for addition.

DISCUSSION

The recently determined crystal structure of human Thg1 provided the long-awaited opportunity to investigate the molecular mechanism of the unusual 3′−5′ nucleotide addition reaction catalyzed by Thg1 enzymes, yet even with these structural data, many questions regarding the roles of Thg1 residues in the individual steps of 3′−5′ nucleotide addition remain unanswered. In addition, there is a clear need for a detailed kinetic analysis to address these questions in light of the ambiguity of the structural data. In this study, we used single-turnover kinetics to individually probe the three known chemical steps of the eukaryotic $tRNA^{His}$ G_{-1} addition reaction (Figures 1−5 and Table 1). Using the kinetic framework we established, we provide support for the proposed position of the 5′ end activating ATP nucleotide (Table 2 and Figures 6 and 7). We also identify previously unknown roles for Thg1 active site residues in the nucleotidyl transfer and pyrophosphate removal steps of the G_{-1} addition reaction. These include a critical role for the two metal-coordinating carboxylate residues in all three chemical steps of G_{-1} addition, and the likely role of three highly conserved positively charged residues in the nucleotidyl transfer step of the reaction, possibly through positioning the incoming NTP to be added to the 5′ end of the polynucleotide chain. Our data provide insight into the mechanism of 3′−5′ addition catalyzed by Thg1 and are the foundation for investigating additional 3′−5′ addition activities catalyzed by other Thg1 family enzymes, including tRNA editing and repair reactions.

The crystal structure of hThg1 revealed a $\beta\alpha\beta\beta\alpha\beta$ motif structurally homologous to the palm domain found in A family DNA polymerases (i.e., T7 DNA pol).[20,27] As observed for A family DNA polymerases, present within this motif are two divalent metal ions coordinated by two highly conserved aspartate residues (D29 and D76) in a bidentate manner (Figure 6). Interestingly, in addition to the 3′−5′ nucleotidyl transfer reaction (Figure 1) that is most analogous to canonical polymerase chemistry, the kinetic data support the hypothesis that the two metal ions are also used by Thg1 to catalyze the adenylylation step and removal of pyrophosphate during G_{-1} addition, based on the deleterious effects of mutation of the metal-coordinating aspartates on all three steps of the reaction. Further analysis will be required to decisively demonstrate the catalytic role of the two metal ions. Parallels may be drawn between the predicted use of a two-metal ion active site to catalyze different chemical transformations by Thg1 and the distinct nucleotide addition and proofreading exonuclease activities proposed to occur within a single two-metal ion active site in some RNA polymerases.[29] However, unlike for RNA polymerases, where the exonuclease activity is the reverse of the addition reaction, the orientation of substrates and reactive phosphates with respect to the two metal ions is predictably different for each of the different steps of G_{-1} addition by Thg1. Therefore, conformational changes during the course of the reaction are necessarily expected to occur, just as are observed for canonical 5′−3′ polymerases.[30−33]

In the hThg1 structure, both metals contact the bound nucleotide proposed to mimic the position of the activating

ATP.[20] Though activation of the nucleophilic 5′ terminal phosphate of the tRNA may not be required for attack on the α-phosphate of the ATP, by analogy to canonical polymerases it is possible that metal A may serve this function in addition to stabilizing the pentacovalent transition state, while metal B participates in transition-state stabilization and promotes the pyrophosphate leaving group.[21] The adenylylation step of 3′−5′ nucleotide addition strongly resembles the activation step of a ligation reaction catalyzed by DNA/RNA ligases. Though ligases require divalent cations for catalysis and two divalent metals are seen in the T4 RNA ligase active site, mutational analysis of the metal binding residues argues against a classical two-metal ion mechanism as with polymerases.[34] Furthermore, under the reaction conditions used in our assays, formation of a covalent AMP−enzyme intermediate, a shared mechanistic feature among all known covalent nucleotidyl transferase enzymes (i.e., ligase and mRNA capping enzymes), is not observed.[35−37] Therefore, Thg1 is to the best of our knowledge the only enzyme that appears to utilize a two-metal ion mechanism to catalyze the activation of the 5′ terminal phosphate of a polynucleotide chain via formation of a 5′−5′ phosphoanhydride bond.

Notably, for several variants, substantial defects in the maximal pseudo-first-order rate constants were observed upon alteration of the side chain to alanine (Table 2), despite the fact that direct roles in the chemistry of the reaction are not obvious from the currently available structural data. For example, the R27, R133, and K96 residues implicated in the nucleotidyl transfer step are all observed to bind the triphosphate moiety of the second bound nucleotide (Figure 6), whereas the 3′-hydroxyl of this nucleotide (not visible in the existing hThg1 structure) is the reactive group for this step. Additionally, the observation of smaller but significant defects in k_{aden} for the R27, R133, and K96 variants supports the idea that the overall organization of the Thg1 active site, including positioning the reactive tRNA substrate, is important for efficient catalysis, yet no structural data are available to indicate the position of bound tRNA in the active complex for catalysis. Similarly, K44 and N161 exhibit strong defects in adenylylation (Figure 7) but, in our structure, are not close enough to make direct contacts with the bound nucleotide that mimics the activating ATP (Figure 6). In the absence of structures that provide insight into the multiple distinct steps that occur during 3′−5′ addition, the kinetic data are essential to understanding the mechanism of this unusual reaction. Furthermore, although the nature of the rate-determining step for k_{max} for each of the three steps is not yet known, these observations strongly support the idea that the measured k_{max} values may reflect rate-determining conformational rearrangements necessary for catalysis, instead of the rates of the actual chemical steps.

The kinetic data suggest that the active site metals may participate in the removal of pyrophosphate from the 5′ end of the G_{-1}-containing tRNA (Table 2 and Figure 7), presumably by activating a nucleophilic water molecule. This reaction is similar to the divalent cation-dependent hydrolysis reaction catalyzed by the bacterial pyrophosphohydrolase RppH that hydrolyzes pyrophosphate from the 5′-triphosphate of mRNAs in prokaryotes, initiating mRNA decay.[38,39] RppH belongs to the Nudix superfamily that includes orthologs in eukaryotes (Dcp2) that catalyze decapping of deadenylylated mRNAs.[40] Mechanisms proposed for Nudix enzymes implicate a protein side chain as a general base in the deprotonation of a metal-activated water for the hydrolysis reaction. Our mutational analysis has not thus far revealed evidence of a general base that could participate in this step of the G_{-1} addition reaction. Alternatively, in the absence of a general base, the water nucleophile may be coordinated by metal A and the tRNA. The possibility that metal A alone may be sufficient for this step of the 3′−5′ addition reaction has precedence in the ribonuclease RNase H, where, in addition to metal A, the proposed nucleophilic water is coordinated by the nonbridging oxygen of the phosphate 3′ to the scissile bond of the nucleic acid substrate.[41,42] However, in the absence of structural information to define the orientation of tRNA in the active site, the orientation of the metals with respect to the 5′ end of the tRNA remains uncertain and, moreover, may change during the course of the reaction cycle.

Comparison of steady-state and single-turnover kinetic parameters shows that k_{aden} is the slowest of the three chemical steps measured here at pH 7.5, and the lower limit to this rate constant observed here (>0.06 min^{-1}) is not substantially different from the measured k_{cat} for p-$tRNA^{His}$ (0.012 min^{-1}) previously determined at the same pH.[16] Therefore, adenylylation may be the rate-determining step for yThg1-catalyzed addition of G_{-1} to p-$tRNA^{His}$ at pH 7.5 under multiple-turnover conditions. Because the adenylylation step is bypassed by the use of ppp-tRNA (Figure 1B), a different step must be rate-determining for multiple-turnover G_{-1} addition with this substrate, but the identity of that step cannot be determined from these data. The previously measured steady-state k_{cat} at pH 7.5 (0.14 min^{-1}) is significantly slower than the values of k_{ntrans} and k_{ppase} measured in the presence of GTP, suggesting neither of these is rate-limiting (Table 1). Therefore, k_{cat} for addition to ppp-$tRNA^{His}$ may reflect either a rate-limiting conformational change that cannot be detected with our single-turnover assays or perhaps product release.

This study provides the first kinetic insight into the individual steps of the non-WC addition of G_{-1} to $tRNA^{His}$, the known physiological function of Thg1 in yeast, yet Thg1 family enzymes are implicated in additional activities, including tRNA 5′ editing and tRNA repair.[13,19] These functions require Thg1 to take advantage of its unique ability to catalyze a second, distinct, 3′−5′ polymerase activity. The WC addition activity of Thg1, first discovered in yeast using $tRNA^{His}$ variant substrates but now shown to be a fundamental property of all Thg1 family enzymes,[14,18] is the reverse reaction of the canonical 5′−3′ nucleic acid synthesis reactions catalyzed by all known DNA/RNA polymerases.

The 3′−5′ polymerase activity imposes additional requirements on the Thg1 mechanism that are potentially distinct from those studied here for the non-WC $tRNA^{His}$ maturation reaction. For instance, rather than removing pyrophosphate from a 5′ pppG_{-1}:C_{73} WC base pair created by addition of the first G_{-1} nucleotide during 3′−5′ polymerization, yThg1 utilizes the activated 5′-triphosphorylated end generated by the addition of the G_{-1} nucleotide for subsequent addition reactions.[18] Thus, efficient removal of the pyrophosphate would predictably impede the polymerase reaction, and the mechanistic basis for this difference is unknown. Likewise, because 3′−5′ polymerization does not require reactivation of the 5′ end during multiple rounds of nucleotide addition, the mechanism of the adenylylation reaction may differ for TLPs (from archaea and bacteria) that conducted only WC-dependent polymerase activities as compared with the eukaryotic Thg1 enzymes investigated in this study.[13,14]

Interestingly, in contrast to yThg1, hThg1 contains a putative N-terminal mitochondrial targeting peptide and mitochondrial $tRNA^{His}$ lacks genomically encoded G_{-1} and contains a C_{73}. Consequently, it is likely that human Thg1 catalyzes both non-WC addition to cytosolic A_{73}-containing $tRNA^{His}$ and addition of templated G_{-1} to mitochondrial C_{73}-containing $tRNA^{His}$ substrates in vivo, raising the question of whether hThg1 adds multiple G residues to mito-C_{73} $tRNA^{His}$ in vivo. Further studies will be needed to determine the mechanistic differences, if any, that exist between Thg1 orthologs causing these enzymes to avoid polymerizing multiple G residues to the 5′ end of the tRNA. This question is especially intriguing when considering TLPs from other organisms that have roles in tRNA repair and editing that require multiple additions to C_{73}-containing $tRNA^{His}$ and other tRNA substrates in vivo.

■ ASSOCIATED CONTENT

Supporting Information

Adenylylation kinetics demonstrating the yThg1 concentration dependence at pH 7.5 (Figure S1) and the ATP concentration dependence at pH 6.0 (Figure S2), nucleotidyl transfer kinetics for the GTP concentration dependence at pH 7.5 (Figure S3), and kinetic analysis of the S76A yThg1 variant (Figure S4). This material is available free of charge via the Internet at http://pubs.acs.org.

■ AUTHOR INFORMATION

Corresponding Author

*Department of Biochemistry, 484 W. 12th Ave., Columbus, OH 43210. Phone: (614) 247-8097. Fax: (614) 292-6773. E-mail: jackman.14@osu.edu.

Funding

This research was supported by National Institutes of Health Grant GM08543 (to J.E.J.).

■ ACKNOWLEDGMENTS

We are grateful to Sam Hyde and Sylvie Doublié for helpful discussions and assistance with preparation of the hThg1 structure figure and Bhalchandra Rao for comments and help with preparation of the manuscript.

■ ABBREVIATIONS

HisRS, histidyl-tRNA synthetase; Thg1, $tRNA^{His}$ guanylyltransferase; TLPs, Thg1-like proteins; p-$tRNA^{His}$, 5′-monophosphorylated $tRNA^{His}$; ppp-$tRNA^{His}$, 5′-triphosphorylated $tRNA^{His}$; WC, Watson−Crick; DTT, dithiothreitol; EDTA, ethylenediaminetetraacetic acid; HEPES, 4-(2-hydroxyethyl)-1-piperazineethanesulfonic acid; Bis-Tris, [bis(2-hydroxyethyl)-amino]-2-(hydroxymethyl)propane-1,3-diol; Tris, 2-amino-2-(hydroxymethyl)propane-1,3-diol; RNase A, ribonuclease A.

■ REFERENCES

(1) Giege, R., Sissler, M., and Florentz, C. (1998) Universal rules and idiosyncratic features in tRNA identity. *Nucleic Acids Res. 26*, 5017−5035.

(2) Nameki, N., Asahara, H., Shimizu, M., Okada, N., and Himeno, H. (1995) Identity elements of *Saccharomyces cerevisiae* tRNA(His). *Nucleic Acids Res. 23*, 389−394.

(3) Rudinger, J., Felden, B., Florentz, C., and Giege, R. (1997) Strategy for RNA recognition by yeast histidyl-tRNA synthetase. *Bioorg. Med. Chem. 5*, 1001−1009.

(4) Rudinger, J., Florentz, C., and Giege, R. (1994) Histidylation by yeast HisRS of tRNA or tRNA-like structure relies on residues −1 and 73 but is dependent on the RNA context. *Nucleic Acids Res. 22*, 5031−5037.

(5) Himeno, H., Hasegawa, T., Ueda, T., Watanabe, K., Miura, K., and Shimizu, M. (1989) Role of the extra G-C pair at the end of the acceptor stem of tRNA(His) in aminoacylation. *Nucleic Acids Res. 17*, 7855−7863.

(6) Rosen, A. E., Brooks, B. S., Guth, E., Francklyn, C. S., and Musier-Forsyth, K. (2006) Evolutionary conservation of a functionally important backbone phosphate group critical for aminoacylation of histidine tRNAs. *RNA 12*, 1315−1322.

(7) Rosen, A. E., and Musier-Forsyth, K. (2004) Recognition of G-1:C73 atomic groups by *Escherichia coli* histidyl-tRNA synthetase. *J. Am. Chem. Soc. 126*, 64−65.

(8) Orellana, O., Cooley, L., and Soll, D. (1986) The additional guanylate at the 5′ terminus of *Escherichia coli* tRNAHis is the result of unusual processing by RNase P. *Mol. Cell. Biol. 6*, 525−529.

(9) Cooley, L., Appel, B., and Soll, D. (1982) Post-transcriptional nucleotide addition is responsible for the formation of the 5′ terminus of histidine tRNA. *Proc. Natl. Acad. Sci. U.S.A. 79*, 6475−6479.

(10) Gu, W., Jackman, J. E., Lohan, A. J., Gray, M. W., and Phizicky, E. M. (2003) tRNAHis maturation: An essential yeast protein catalyzes addition of a guanine nucleotide to the 5′ end of tRNAHis. *Genes Dev. 17*, 2889−2901.

(11) Gu, W., Hurto, R. L., Hopper, A. K., Grayhack, E. J., and Phizicky, E. M. (2005) Depletion of *Saccharomyces cerevisiae* tRNA(His) guanylyltransferase Thg1p leads to uncharged tRNAHis with additional m_5C. *Mol. Cell. Biol. 25*, 8191−8201.

(12) Preston, M. A., and Phizicky, E. M. (2010) The requirement for the highly conserved G-1 residue of *Saccharomyces cerevisiae* tRNAHis can be circumvented by overexpression of tRNAHis and its synthetase. *RNA 16*, 1068−1077.

(13) Rao, B. S., Maris, E. L., and Jackman, J. E. (2011) tRNA 5′-end repair activities of tRNAHis guanylyltransferase (Thg1)-like proteins from Bacteria and Archaea. *Nucleic Acids Res. 39*, 1833−1842.

(14) Abad, M. G., Rao, B. S., and Jackman, J. E. (2010) Template-dependent 3′-5′ nucleotide addition is a shared feature of tRNAHis guanylyltransferase enzymes from multiple domains of life. *Proc. Natl. Acad. Sci. U.S.A. 107*, 674−679.

(15) Heinemann, I. U., Randau, L., Tomko, R. J. Jr., and Soll, D. (2010) 3′-5′ tRNAHis guanylyltransferase in bacteria. *FEBS Lett. 584*, 3567−3572.

(16) Jackman, J. E., and Phizicky, E. M. (2006) tRNAHis guanylyltransferase adds G-1 to the 5′ end of tRNAHis by recognition of the anticodon, one of several features unexpectedly shared with tRNA synthetases. *RNA 12*, 1007−1014.

(17) Jahn, D., and Pande, S. (1991) Histidine tRNA guanylyltransferase from *Saccharomyces cerevisiae*. II. Catalytic mechanism. *J. Biol. Chem. 266*, 22832−22836.

(18) Jackman, J. E., and Phizicky, E. M. (2006) tRNAHis guanylyltransferase catalyzes a 3′-5′ polymerization reaction that is distinct from G-1 addition. *Proc. Natl. Acad. Sci. U.S.A. 103*, 8640−8645.

(19) Abad, M. G., Long, Y., Willcox, A., Gott, J. M., Gray, M. W., and Jackman, J. E. (2011) A role for tRNA(His) guanylyltransferase (Thg1)-like proteins from *Dictyostelium discoideum* in mitochondrial 5′-tRNA editing. *RNA 17*, 613−623.

(20) Hyde, S. J., Eckenroth, B. E., Smith, B. A., Eberley, W. A., Heintz, N. H., Jackman, J. E., and Doublie, S. (2010) tRNAHis guanylyltransferase (THG1), a unique 3′-5′ nucleotidyl transferase, shares unexpected structural homology with canonical 5′-3′ DNA polymerases. *Proc. Natl. Acad. Sci. U.S.A. 107*, 20305−20310.

(21) Steitz, T. A. (1998) A mechanism for all polymerases. *Nature 391*, 231−232.

(22) Steitz, T. A. (1999) DNA polymerases: Structural diversity and common mechanisms. *J. Biol. Chem. 274*, 17395−17398.

(23) Jackman, J. E., and Phizicky, E. M. (2008) Identification of critical residues for G-1 addition and substrate recognition by tRNA(His) guanylyltransferase. *Biochemistry 47*, 4817−4825.

(24) Fierke, C. A., and Hammes, G. G. (1995) Transient kinetic approaches to enzyme mechanisms. *Methods Enzymol. 249*, 3−37.
(25) Sohn, J., Buhrman, G., and Rudolph, J. (2007) Kinetic and structural studies of specific protein-protein interactions in substrate catalysis by Cdc25B phosphatase. *Biochemistry 46*, 807−818.
(26) Doublie, S., and Ellenberger, T. (1998) The mechanism of action of T7 DNA polymerase. *Curr. Opin. Struct. Biol. 8*, 704−712.
(27) Doublie, S., Tabor, S., Long, A. M., Richardson, C. C., and Ellenberger, T. (1998) Crystal structure of a bacteriophage T7 DNA replication complex at 2.2 Å resolution. *Nature 391*, 251−258.
(28) Polesky, A. H., Dahlberg, M. E., Benkovic, S. J., Grindley, N. D., and Joyce, C. M. (1992) Side chains involved in catalysis of the polymerase reaction of DNA polymerase I from *Escherichia coli*. *J. Biol. Chem. 267*, 8417−8428.
(29) Sydow, J. F., and Cramer, P. (2009) RNA polymerase fidelity and transcriptional proofreading. *Curr. Opin. Struct. Biol. 19*, 732−739.
(30) Vaisman, A., Ling, H., Woodgate, R., and Yang, W. (2005) Fidelity of Dpo4: Effect of metal ions, nucleotide selection and pyrophosphorolysis. *EMBO J. 24*, 2957−2967.
(31) Franklin, M. C., Wang, J. M., and Steitz, T. A. (2001) Structure of the replicating complex of a pol alpha family DNA polymerase. *Cell 105*, 657−667.
(32) Beard, W. A., and Wilson, S. H. (1998) Structural insights into DNA polymerase β fidelity: Hold tight if you want it right. *Chem. Biol. 5*, R7−R13.
(33) Doublié, S., Sawaya, M. R., and Ellenberger, T. (1999) An open and closed case for all polymerases. *Structure 7*, R31−R35.
(34) Wang, L. K., Schwer, B., and Shuman, S. (2006) Structure-guided mutational analysis of T4 RNA ligase 1. *RNA 12*, 2126−2134.
(35) Shuman, S. (2001) Structure, mechanism, and evolution of the mRNA capping apparatus. *Prog. Nucleic Acid Res. Mol. Biol. 66*, 1−40.
(36) Shuman, S., and Hurwitz, J. (1981) Mechanism of mRNA capping by vaccinia virus guanylyltransferase: Characterization of an enzyme−guanylate intermediate. *Proc. Natl. Acad. Sci. U.S.A. 78*, 187−191.
(37) Shuman, S., and Schwer, B. (1995) RNA capping enzyme and DNA ligase: A superfamily of covalent nucleotidyl transferases. *Mol. Microbiol. 17*, 405−420.
(38) Deana, A., Celesnik, H., and Belasco, J. G. (2008) The bacterial enzyme RppH triggers messenger RNA degradation by 5′ pyrophosphate removal. *Nature 451*, 355−358.
(39) Messing, S. A., Gabelli, S. B., Liu, Q., Celesnik, H., Belasco, J. G., Pineiro, S. A., and Amzel, L. M. (2009) Structure and biological function of the RNA pyrophosphohydrolase BdRppH from *Bdellovibrio bacteriovorus*. *Structure 17*, 472−481.
(40) Wang, Z., Jiao, X., Carr-Schmid, A., and Kiledjian, M. (2002) The hDcp2 protein is a mammalian mRNA decapping enzyme. *Proc. Natl. Acad. Sci. U.S.A. 99*, 12663−12668.
(41) Nowotny, M., Gaidamakov, S. A., Crouch, R. J., and Yang, W. (2005) Crystal structures of RNase H bound to an RNA/DNA hybrid: Substrate specificity and metal-dependent catalysis. *Cell 121*, 1005−1016.
(42) Nowotny, M., and Yang, W. (2006) Stepwise analyses of metal ions in RNase H catalysis from substrate destabilization to product release. *EMBO J. 25*, 1924−1933.